





Structural characterization of proton-pumping rhodopsin lacking a cytoplasmic proton donor residue by X-ray crystallography

Received for publication, January 11, 2022, and in revised form, February 5, 2022. Published, Papers in Press, February 11, 2022.

<https://doi.org/10.1016/j.jbc.2022.101722>

Kano Suzuki^{1,‡}, María del Carmen Marín^{2,‡} , Masae Konno^{2,3,‡} , Reza Bagherzadeh², Takeshi Murata^{1,4,*}, and Keiichi Inoue^{2,*}

From the ¹Department of Chemistry, Graduate School of Science, Chiba University, Inage, Chiba, Japan; ²The Institute for Solid State Physics, The University of Tokyo, Kashiwa, Chiba, Japan; ³PRESTO, Japan Science and Technology Agency, Kawaguchi, Saitama, Japan; ⁴Membrane Protein Research and Molecular Chirality Research Centers, Chiba University, Inage, Chiba, Japan

Edited by Wolfgang Peti

DTG/DTS rhodopsin, which was named based on a three-residue motif (DTG or DTS) that is important for its function, is a light-driven proton-pumping microbial rhodopsin using a retinal chromophore. In contrast to other light-driven ion-pumping rhodopsins, DTG/DTS rhodopsin does not have a cytoplasmic proton donor residue, such as Asp, Glu, or Lys. Because of the lack of cytoplasmic proton donor residue, proton directly binds to the retinal chromophore from the cytoplasmic solvent. However, mutational experiments that showed the complicated effects of mutations were not able to clarify the roles played by each residue, and the detail of proton uptake pathway is unclear because of the lack of structural information. To understand the proton transport mechanism of DTG/DTS rhodopsin, here we report the three-dimensional structure of one of the DTG/DTS rhodopsins, *PspR* from *Pseudomonas putida*, by X-ray crystallography. We show that the structure of the cytoplasmic side of the protein is significantly different from that of bacteriorhodopsin, the best-characterized proton-pumping rhodopsin, and large cytoplasmic cavities were observed. We propose that these hydrophilic cytoplasmic cavities enable direct proton uptake from the cytoplasmic solvent without the need for a specialized cytoplasmic donor residue. The introduction of carboxylic residues homologous to the cytoplasmic donors in other proton-pumping rhodopsins resulted in higher pumping activity with less pH dependence, suggesting that DTG/DTS rhodopsins are advantageous for producing energy and avoiding intracellular alkalization in soil and plant-associated bacteria.

Microbial rhodopsins are a large family of photoreceptive heptahelical transmembrane (TM) proteins (1–3). They share a common structural architecture consisting of seven TM helices (TM1–7) and an all-*trans*-retinal chromophore, which is covalently connected to a conserved lysine *via* a protonated

Schiff base linkage. More than 10,000 microbial rhodopsins have been identified by genomic and metagenomic analyses of diverse microorganisms (bacteria, archaea, algae, fungi, protists, etc.) as well as in giant viruses (2–6). Light absorption by microbial rhodopsin induces the isomerization of the retinal chromophore to the 13-*cis* form and is associated with various types of biological molecular functions, including light-driven ion pumps (6, 7), light-gated channels (8–10), light-dependent gene regulation (11, 12), and light-dependent enzyme (13) (Fig. 1). A new rhodopsin family, heliorhodopsin, which is distinct from all typical microbial rhodopsins and has an inverted protein orientation, was recently discovered (14). However, the function of heliorhodopsin remains unknown.

The most abundant microbial rhodopsin is light-driven outward proton (H⁺)-pumping rhodopsins, which convert light energy to the chemical potential of the H⁺ gradient (proton motive force) to promote ATP synthesis by ATP synthase and other H⁺-coupled transport events (15). The first light-driven outward H⁺ pump, bacteriorhodopsin (BR), was found in the extreme halophilic archaeon *Halobacterium salinarum* (formerly called *Halobacterium halobium*) (16). The photoexcited BR exhibited a cyclic reaction, called a photocycle, composed of several photointermediates. Multistep H⁺ transfer occurs during outward H⁺ pumping, and acidic residues in BR (BR Asp85, Asp96, Glu194, and Glu204) play critical roles (1, 17). First, several tens of microseconds after the photoisomerization of the retinal, H⁺ is transferred from the retinal Schiff base (RSB) to BR Asp85, which is deprotonated and stabilizes the protonated RSB as a counterion in TM3 in the dark state. Then, another proton is released from a complex composed of Glu194, Glu204, and a bound water molecule (proton-release group [PRG]) to extracellular solvent (18, 19). Next, H⁺ is transferred from the cytoplasmic Asp96 to the deprotonated RSB. Finally, after H⁺ uptake of Asp96 from the cytoplasmic solvent, an H⁺ transfer from Asp85 to PRG occurs at the final step of the photocycle; it has been suggested that Asp212, another counterion in TM7, participates in this long H⁺ transfer (20, 21).

Acidic residues homologous to BR Asp85 and Asp96 are conserved in other H⁺-pumping rhodopsins, whereas PRG is

[‡] These authors contributed equally to this work.

* For correspondence: Keiichi Inoue, inoue@issp.u-tokyo.ac.jp; Takeshi Murata, t.murata@faculty.chiba-u.jp.

X-ray crystallographic structure of DTG/DTS rhodopsin

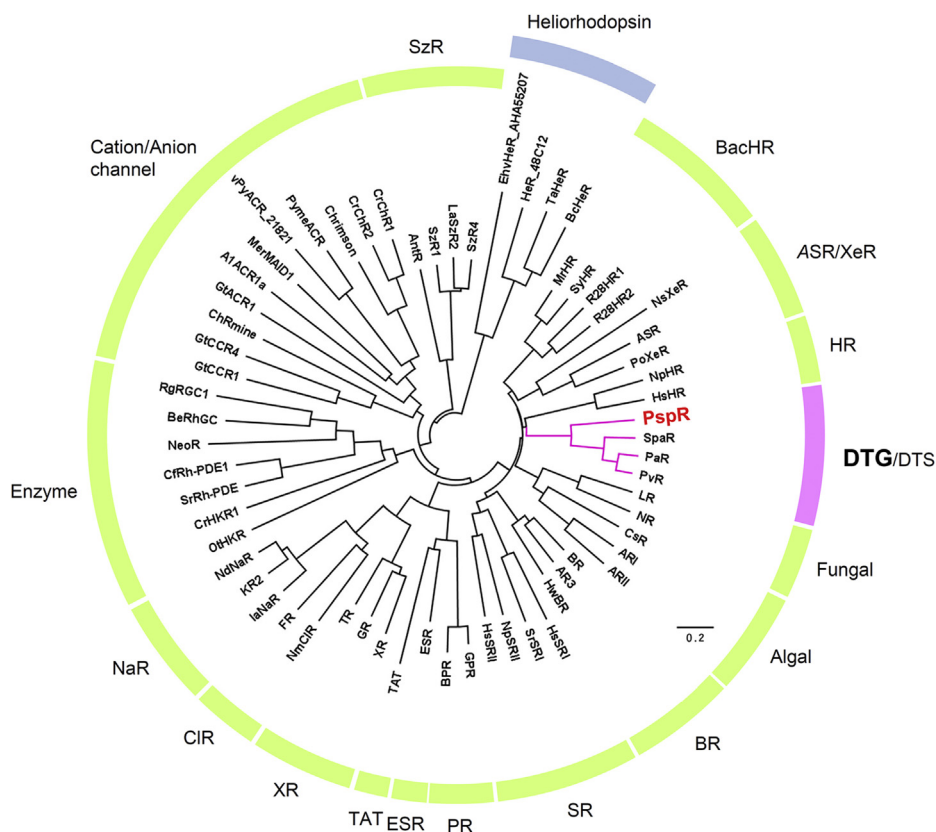


Figure 1. Phylogenetic tree of microbial rhodopsins. A phylogenetic tree of type 1 microbial rhodopsins (green) and heliorhodopsin (blue). The branches of DTG/DTS rhodopsins are indicated by magenta, and *PspR* is indicated by red bold letters. *PspR*, DTG rhodopsin from *Pseudomonas putida*.

not necessarily conserved. These two residues and BR Thr89, which are also important for the H⁺-pumping function, are called the DTD motif (7, 22). In other outward H⁺-pumping rhodopsins from bacteria, called proteorhodopsin and xanthorhodopsins, BR Asp96 is substituted with a glutamic acid residue (DTE motif) (23, 24). In addition, *Exiguobacterium sibiricum* rhodopsin uses lysine residue as a nonacidic H⁺ donor (DTK motif) (25). In contrast to these outward H⁺-pumping rhodopsins, a new family of outward H⁺-pumping rhodopsins without a cytoplasmic donor residue was found (26, 27). In these rhodopsins, glycine residue is in a position homologous to BR Asp96, giving rise to their name “DTG rhodopsin” (Fig. S1) (3, 6). Another outward H⁺-pumping rhodopsin, *SpaR*, is phylogenetically very close to DTG rhodopsin but has a serine residue at the position homologous to BR Asp96 (DTS motif) (28). Therefore, we refer to these rhodopsins without a cytoplasmic donor as “DTG/DTS rhodopsin.” Owing to the lack of a cytoplasmic donor, H⁺ directly binds from the cytoplasmic solvent to the RSB, so that the rate of reprotonation is proportional to the external H⁺ concentration (26, 27). On the other hand, it has been argued that a conserved histidine residue at the position of BR Thr46 in TM2 works as a new proton donor. Although the mutations of this histidine residue in the best-characterized DTG rhodopsin from *Pseudomonas putida*, *PspR*, to an arginine residue or a tyrosine residue (*PspR* H37R and H37Y) slowed down the reprotonation of RSB, no significant effect

was observed for a histidine-to-asparagine (H37N) mutant. The complex results of the histidine mutants suggest that the proton-uptake process of DTG/DTS rhodopsins is not a simple event and that a more complex mechanism is involved. To understand the mechanism of H⁺ uptake by DTG/DTS rhodopsins in detail, we performed a three-dimensional structural analysis of *PspR* using X-ray crystallographic analysis.

Results

The X-ray crystallographic structure of *PspR* was obtained at 2.84 Å resolution using the lipidic cubic phase (LCP) method (Fig. 2 and Table S1). In the crystal, *PspR* showed a trimeric structure similar to that of BR (Fig. 2A). Whereas the cytoplasmic side of TM5 of *PspR* is shorter than that of BR by two α-helical turns, other parts of the TM of *PspR* overlap well with the structure of BR (Fig. 2B). However, the cytoplasmic side of the TMs of *PspR* was significantly displaced from that of BR (Fig. 2B, blue arrows), whereas no large displacement was observed on the extracellular side. This structural difference on the cytoplasmic side is related to the rearrangement of the structure because of the loss of cytoplasmic donor in *PspR*. In particular, the cytoplasmic side of TM7 from *PspR* Ala212–Arg222 moves away from TM1, creating larger cytoplasmic cavities compared with BR (Fig. 2C, dashed circles). These cytoplasmic cavities would increase the accessibility of water from the cytoplasmic milieu to the RSB region and would be

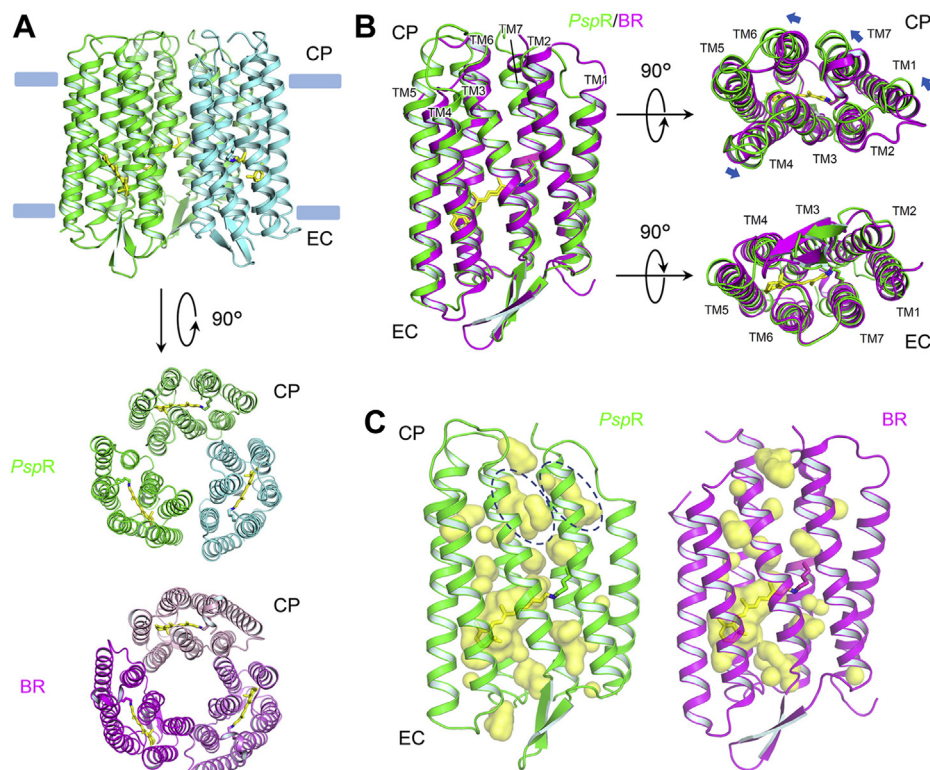


Figure 2. X-ray crystallographic structure of PspR. A, trimer of PspR viewed from the direction parallel to the lipid bilayer (top) and from the cytoplasmic side (CS; middle). Trimers of BR (Protein Data Bank ID: 1M0L (63)) viewed from the CS (bottom). The approximate position of the membrane surface is shown by blue rectangles. B, overlaid structures of PspR (green) and BR (magenta). C, cavities (pale yellow) in PspR (green) and BR (purple). The cytoplasmic cavities specific to PspR, but not in BR, are indicated by dashed circles. BR, bacteriorhodopsin; EC, extracellular side; PspR, DTG rhodopsin from *Pseudomonas putida*.

related to the direct binding of H⁺ to the RSB at the last stage of the photocycle.

Similar to many outward H⁺-pumping rhodopsins, the H⁺ transport pathway of PspR is thought to exist in the hydrophilic interhelical region surrounded by TM2, TM3, TM6, and TM7, including the RSB-binding site (1, 17, 26, 29–34). Hence, we focused on the amino acid residues consisting of this interhelical region (Fig. 3). Two carboxylates (PspR Asp73 and Asp206) (Fig. 3B) are present on the extracellular side of the RSB, stabilizing the protonated RSB via electrostatic interactions in the dark. While a hydrogen bond is present between Asp73 and Thr77, Asp206 is also hydrogen bonded with two tyrosine residues, Tyr48 in TM2 and Tyr179 in TM6. These hydrogen bonds are believed to stabilize the negative charges of the counterions. In BR, homologous counterions are bridged by three internal water molecules (Wat401, 402, and 406) (Fig. 3B, right) with protonated RSB, Thr89, and Arg82. In contrast, two water molecules exist in this region in PspR (Wat1 and 2) (Fig. 3B, left). The difference in the numbers of water molecules altered the orientation of the counterions in PspR compared with BR. As a result, the hydrogen-bonding distance between Wat1 and the counterions in PspR is shorter than that between Wat402 and counterions in BR, whereas the distance between Asp73 and Thr77 in PspR is longer than that between Asp85 and Thr89 in BR.

In contrast to the high similarity of the RSB region between PspR and BR, a significant difference was observed on the

extracellular side. In BR, Glu194 and Glu204 make the PRG with water molecules on the extracellular surface (Fig. 3C, bottom). BR Glu204 is substituted with Thr198 in PspR, and the PspR Glu188 homologous to BR Glu194 forms a different type of hydrogen bond with Arg70, Tyr71, and a water molecule (Fig. 3C, top), suggesting that the H⁺ release process of PspR would be different from BR. To investigate the role of PspR Glu188 in the H⁺ release process, we measured the H⁺-pumping activity of PspR E188Q and E188A. The pumping activities of PspR E188A and E188Q were 35% to 40% of PspR WT (Fig. 4), suggesting the significance of Glu188 in the proton release process of PspR.

The cytoplasmic cavity of the interhelical region surrounded by TM2, TM3, TM6, and TM7 consists of many hydrophilic residues (His33, His37, Tyr91, Tyr213, and Ser217). This is in contrast with BR, in which the cytoplasmic region is more tightly packed by hydrophobic residues in the dark (35). A water molecule was observed near Gly84 (“G” of DTG motif) (Fig. 3D). This water molecule formed hydrogen bonds with two histidine residues, His33 and His37, characteristic of DTG/DTS rhodopsins in TM2 and Tyr213 in TM7. Interestingly, His37 forms two more hydrogen-bonding networks: His37–water–main-chain carbonyl of Lys210 and His37–Ser217. Ser217 is not highly conserved (an alanine is most conserved in DTG/DTS rhodopsins at this position), whereas Tyr213 is conserved in 95% DTG/DTS rhodopsins (Fig. S2). Looking the residue at this position in other microbial

X-ray crystallographic structure of DTG/DTS rhodopsin

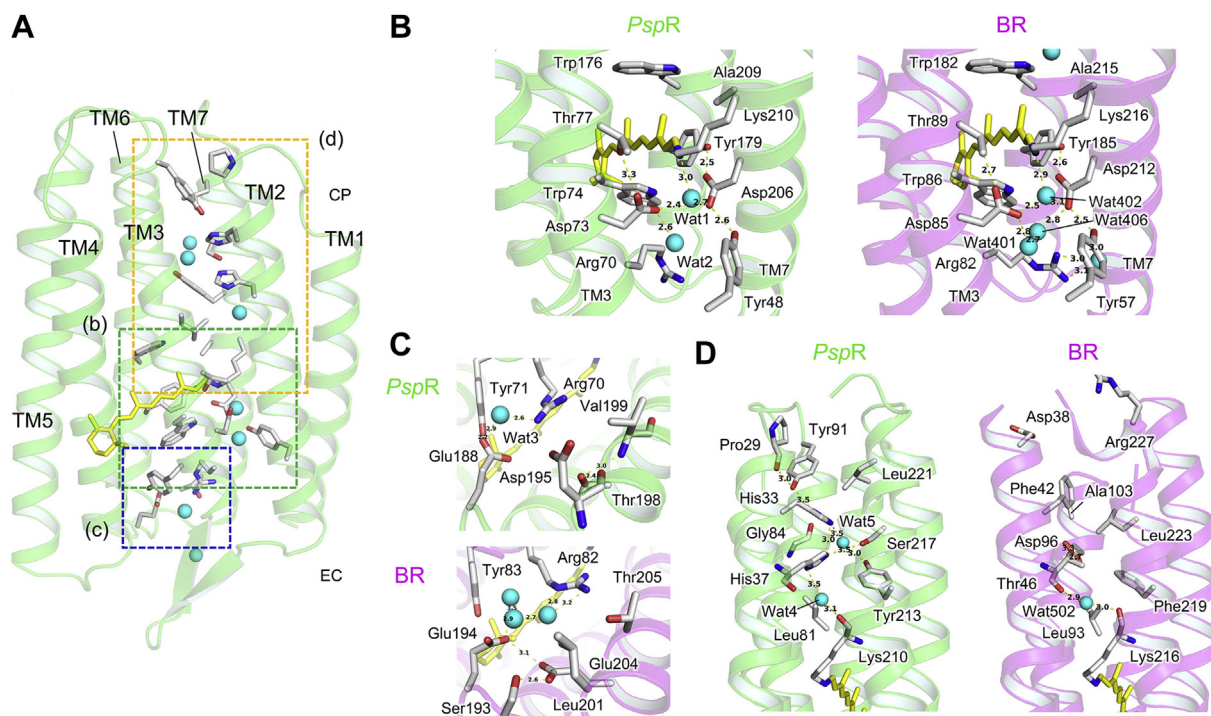


Figure 3. Ion-transport pathway in PspR. A, residues on the putative ion transport pathway in PspR. The regions focused on in B–D are indicated by green, blue, and yellow rectangles, respectively. B, RSB region in PspR (left) and BR (right, Protein Data Bank [PDB] ID: 1M0L (63)). C, the structure of putative PRG in PspR (top) and BR (bottom, PDB ID: 1M0L (63)) viewed from the extracellular side. D, residues constituting the H⁺ uptake pathway from the cytoplasmic surface to the RSB in PspR (left) and BR (right, PDB ID: 1M0L (63)). BR, bacteriorhodopsin; PRG, proton-release group; PspR, DTG rhodopsin from *Pseudomonas putida*; RSB, retinal Schiff base.

rhodopsins, a phenylalanine is present in BR (Phe219), and a homologous tyrosine is conserved only in sodium pump rhodopsins in addition to DTG/DTS rhodopsins. We expected that the Tyr213 characteristic of DTG/DTS rhodopsins would play an important role in its H⁺-pumping function and compared the H⁺-pumping activity of PspR Y213F and Y213A mutants with that of the PspR WT. The activities of these mutants, however, were almost identical to the WT (Fig. 4, A and B). Therefore, Tyr213 would not be critical for H⁺ uptake by PspR. To obtain further insights into this residue, we carried out a laser flash photolysis experiment to determine the photocycles of these mutants. As a result, the photocycle of PspR Y213F was also similar to that of the WT, whereas the decay of the M₂ intermediate representing the deprotonated state of RSB was significantly slower (Fig. 4C). Hence, Tyr213 appears to partly contribute to the acceleration of the H⁺-uptake process of PspR, but it is not critical to generate substantial differences in the activity.

PspR Leu81 in TM3 is completely conserved in DTG/DTS rhodopsins (Fig. S2) and is located near the water molecule connecting His37 and the main-chain carbonyl of Lys210 (Fig. 3D). This leucine residue is also conserved in many other microbial rhodopsins. The mutation of homologous leucine residue in BR (Leu93) slows the photocycle by two orders of magnitude (36). In addition, cryotrapping and femtosecond time-resolved X-ray crystallographic structural analyses have observed the rotation of the side chain of Leu93 during the photocycle (37, 38). The mutation of homologous leucine

residue in light-driven inward H⁺-pumping rhodopsin, schizorhodopsin, results in the loss of function and direct connection between RSB and cytoplasmic solvent, even in the dark (39). These results indicate the importance of this leucine residue in H⁺ transport. Next, we investigated the effect of the PspR L81A mutation. Unexpectedly, the mutant showed 1.9-fold larger activity than that of PspR WT (Fig. 4). The photocycle of PspR L81A showed a large accumulation of the long-lived O-like intermediate equilibrating with M intermediate (Fig. S3), which is observed with only a small amount of accumulation for the WT (26). The excitation of the O-like intermediate by the long-wavelength component of light could result in a shortcut of the photocycle by the photo-induced conversion from the O to the initial state and a higher turnover rate of the H⁺ pumping. To confirm this hypothesis, the pumping activity of PspR WT and L81A was assayed with a narrower excitation wavelength ($\lambda = 535 \pm 10$ nm), at which the O-like intermediate is not excited. As a result, the pH change induced by PspR L81A was considerably smaller than that induced by WT, indicating that the photoisomerization of the O-like intermediate shortcuts the photocycle and enhances the H⁺-transporting rate (Fig. S3).

Finally, Gly84 was mutated to Asp or Glu, which mimics the carboxylic acid at the proton-donor position in DTD-type and DTE-type H⁺-pumping rhodopsins. Surprisingly, PspR G84D exhibited H⁺-pumping activity significantly higher than that of WT, and the activity of G84E was even stronger (Fig. 4, A and B), suggesting that Asp and Glu can enhance the H⁺-pumping

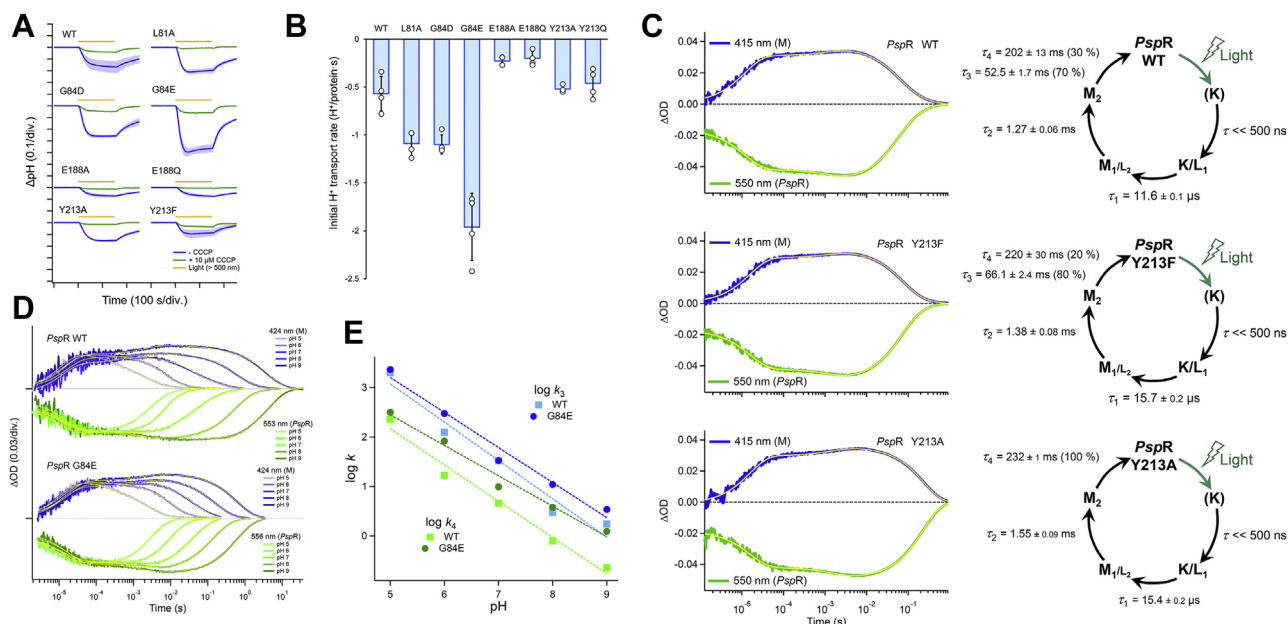


Figure 4. Ion-transport activity and photocycle of *PspR* WT and mutants. *A*, pH changes of the outer solvent in the suspensions of *Escherichia coli* cells expressing *PspR* WT and mutants without (blue) and with (green) 10 μ M CCCP. Light ($\lambda > 500$ nm) was illuminated during the period indicated by yellow bars. The SD of the pH change without CCCP is indicated by light blue area. *B*, initial H^+ transport rates of *PspR* WT and mutants. Data are mean \pm SD. Individual data points are shown by white circles. *C*, transient absorption change (left) and the photocycles (right) of *PspR* WT (top), Y213F (middle), and Y213A (bottom). The protein was reconstituted in POPE/POPG lipid vesicle in 100 mM NaCl and 20 mM HEPES–NaOH (pH 7.0). The transient absorption changes were probed at 415 and 550 nm to observe the accumulation of the M-intermediate and the bleaching of the initial state/accumulation of the L-intermediate, respectively. The decay of the M_2 -intermediate of *PspR* WT and Y213F exhibited two different lifetimes, and the percentages of the pre-exponential factors of each component in the amplitude of the full decay are indicated in parentheses. *D*, transient absorption change of *PspR* WT (upper) and G84E (lower) at different pH. The M-intermediate accumulation and the initial state bleaching were monitored at 424 nm (blue) and 553 or 556 nm (green), respectively. *E*, pH dependence of the rate constants of faster (blue) and slower (green) M decays of *PspR* WT (light-colored squares) and G84E (dark-colored circles). The lifetimes of each photointermediate in the photocycles were determined by global fitting of the transient absorption change with a multiexponential function (left, yellow lines in *C* and *D*). CCCP, carbonyl cyanide *m*-chlorophenylhydrazone; POPE, 1-palmitoyl-2-oleoyl-phosphatidyl-ethanolamine; POPG, 1-palmitoyl-2-oleoyl-*sn*-glycero-3-phosphoglycerol; *PspR*, DTG rhodopsin from *Pseudomonas putida*.

activity compared with natural glycine residue. The transient absorption change of *PspR* G84E was similar to that of the WT (Fig. 4D). Its rate of the decay of the M-intermediate, however, was less dependent on pH, represented by the smaller slopes in Figure 4E than that of the WT; therefore, the turnover rate of the photocycle of *PspR* G84E is faster than that of WT at pH ≥ 7 .

Discussion

DTG/DTS rhodopsins are the first light-driven outward H^+ -pumping rhodopsins without a proton donor residue at a position homologous to BR Asp96 (recently, a viral rhodopsin distant from DTG/DTS rhodopsins with an identical motif was also reported to have an outward H^+ -pumping function (34)). Although a previous study suggested direct H^+ uptake from the cytoplasmic milieu to the RSB and substantial involvement of His37 in this process, no detailed structural insights were obtained.

The X-ray crystallographic structure obtained in this study showed that *PspR* forms a trimer similar to that of BR (Fig. 2A). Halophilic archaeal rhodopsins (BR, sensory rhodopsin, and halorhodopsin) in the phylogenetic tree in Fig. 1) and their close relatives from bacteria, other archaea, and eukaryotes (bacterial halorhodopsin, *Anabaena* sensory rhodopsin/xenorhodopsin, and fungal and algal rhodopsins in

the phylogenetic tree in Fig. 1) are known to exist as trimers (40–43). The DTG/DTS family is phylogenetically close to them, suggesting that these trimeric rhodopsins evolved from a common origin (trimeric ancestor).

The structure of the RSB region in *PspR* is similar to that in BR (Fig. 3B). Previously, the hydrogen-bonding network around the RSB was studied by low-temperature difference FTIR spectroscopy (26). Based on the smaller number of O–D stretching (str.) bands of D_2O observed for *PspR* than that for BR, the number of water molecules around RSB appeared to be smaller in the former. This is consistent with the smaller number (two) of water molecules hydrogen bonding with the RSB and the counterions in the structure of *PspR*, compared with three in BR (Fig. 3B). On the other hand, Dr Kandori and co-workers (44) found that all outward H^+ -pumping rhodopsins have strongly hydrogen-bonded water, which exhibits an O–D str. band at <2400 cm^{-1} , which is critical for the H^+ -pumping function. The O–D str. band of strongly hydrogen-bonded water was observed for both *PspR* and BR. The band of *PspR* appeared at higher wavenumber (2255 cm^{-1}) than that of BR (2171 cm^{-1}) indicates that the hydrogen bond, which was suggested to be between Wat402 and Asp85 in the structure of BR (45), is weaker in *PspR*. The distance between Wat1 (homologous to Wat402 in BR) in *PspR* and Asp73 (2.4 \AA), however, is shorter than Wat402–Asp85 in BR (2.5 \AA). Although this would seem to contradict the result of FTIR, the

X-ray crystallographic structure of DTG/DTS rhodopsin

angle between the RSB–water–counterion of BR (107.6°) is closer to the ideal tetrahedral angle than *PspR* (94.0°) (Fig. S4). This tight angle between the RSB–water–counterion in *PspR* would weaken the hydrogen bond between Wat1 and Asp73.

Although His37 is highly conserved in DTG/DTS rhodopsin, a complicated effect of the mutation was reported previously; whereas, long-lived M-intermediate was observed for *PspR* H37Y and H37R, the H37N mutant showed a photocycle identical to that of the WT. In the structure of *PspR*, many cavities connecting the cytoplasmic surface and the central part of the protein existed around His37 (Fig. 5). Hence, if the tilting of TM6 occurs during the H^+ -uptake process, as observed in BR (46–48), a large amount of water molecules may flow into to enable direct H^+ transfer from the cytoplasmic solvent to the RSB. The photocycle of *PspR* H37N suggests that, even if His37 acts as a proton donor to the RSB like BR Asp96, it has only minor effects. On the other hand, the large decrease in the rate of H^+ binding, that is, the M_2 -decay, observed upon substitution with a large aromatic residue (H37Y) or a large basic residue (H37R) (26), may be caused by the disruption of the hydrogen-bonding network and cytoplasmic cavities to maintain the entrance of water molecules. To prove these hypotheses, structural analysis of the photo-intermediate in the future will give us more direct insight.

The mutation of Gly84 to Asp or Glu, that is, the conversion of the motif to DTD and DTE, resulted in approximately twofold and fourfold increases in activity compared with the WT, respectively (Fig. 4, A and B). The less pH-dependent photocycle of *PspR* G84E and its faster turnover rate at $pH \geq 7$ than that of the WT suggests that the Asp and Glu introduced upon G84D and G84 mutations, respectively, partly function as a proton donor to the RSB, similar to carboxylic proton donors in natural DTD-type and DTE-type proton-pumping rhodopsins, which play a role to keep the rate of H^+ uptake constant over a wide pH range (49). Why does

DTG/DTS rhodopsin have a glycine residue, even though proton donors are advantageous for efficient H^+ pumping? DTG/DTS rhodopsins are found mainly in soil and plant-associated bacteria (26). Their habitats are often alkalized, so that these bacteria use specialized pH-homeostasis systems to avoid intracellular alkalization (50). Although DTD/DTE-type proton-pumping rhodopsins are efficient pumps, they continue to transport H^+ if the cells are illuminated under easily alkalizing conditions (51). In contrast, the H^+ -pumping activity of DTG/DTS rhodopsins strongly depends on the intracellular pH (Fig. 4). As a result, they can regulate their activity to energize the cells under normal conditions and can avoid unnecessary intracellular alkalization in soil and plant-associated bacteria. The proton transport mechanism of *PspR* without the cytoplasmic donor residue altering its activity under different conditions provides new insights into active ion transport by membrane proteins and a new basis for the development of next-generation optogenetic tools, which can control the neural activity with avoiding side effects by strong alkalization of the cell body.

Experimental procedures

Phylogenetic analysis of DTG/DTS rhodopsins

For the phylogenetic analysis of DTG/DTS rhodopsins, the amino acid sequences of 63 microbial rhodopsins (Fig. 1) were aligned by ClustalW (52). The evolutionary history was inferred using the neighbor-joining method (53). The optimal tree with the sum of branch length = 32.89314902 is shown. The tree is drawn to scale, with branch lengths in the same units as those of the evolutionary distances used to infer the phylogenetic tree. The evolutionary distances were computed using the Poisson correction method (54) and are in the units of the number of amino acid substitutions per site. The analysis involved 63 amino acid sequences. All ambiguous positions were removed for each sequence pair. There were a total of 378 positions in the final dataset. Evolutionary analyses were conducted in MEGA6 (Molecular Evolutionary Genetics Analysis, version 6.0) software (55).

Construction of DNA plasmids for the expression of *PspR*

The gene encoding *PspR* with codons optimized for *Escherichia coli* (*E. coli*) expression was synthesized by GenScript and cloned into NdeI–XhoI site of pET21a (+) vector (Novagen, Merck KGaA). The plasmid was transformed into *E. coli* C43 (DE3) strain (Lucigen). For mutagenesis, the QuikChange site-directed mutagenesis method (Agilent Technologies) was used according to a standard protocol. The sequences of the primers used in mutagenesis are listed in Table S2.

Protein expression and purification

E. coli cells harboring the *PspR*-cloned plasmids were cultured in 2× YT medium containing 50 $\mu\text{g/ml}$ ampicillin. The expression of C-terminal 6× His-tagged proteins was induced by 0.1 mM IPTG in the presence of 10 μM all-*trans*-retinal (Toronto Research Chemicals) for 4 h at 37 °C. The

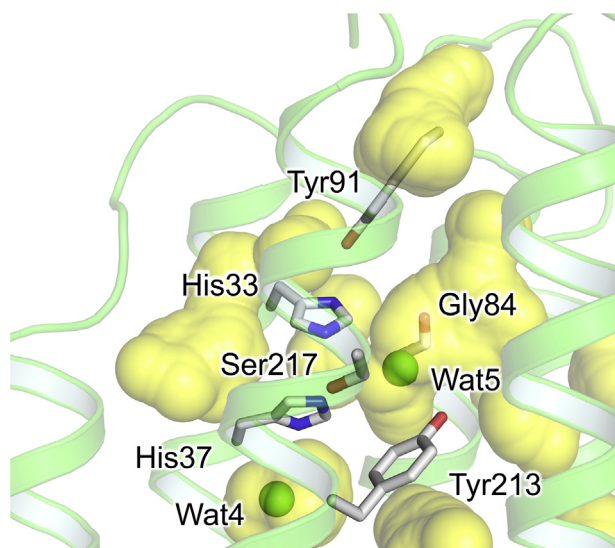


Figure 5. Cavities around *PspR* His37. Cavities around *PspR* His37 on the cytoplasmic side (pale yellow). *PspR*, DTG rhodopsin from *Pseudomonas putida*.

harvested cells were sonicated (Ultrasonic Homogenizer VP-300N; TAITEC) for disruption in buffer containing 50 mM Tris-HCl (pH 8.0) and 5 mM MgCl₂. The membrane fraction was collected by ultracentrifugation (CP80NX; Eppendorf HimaC Technologies) at 142,000g for 1 h. The proteins were solubilized in a buffer containing 50 mM MES-NaOH (pH 6.5), 300 mM NaCl, 5 mM imidazole, 5 mM MgCl₂, and 3% *n*-dodecyl-β-D-maltopyranoside (DDM) (ULTROL Grade; Calbiochem). The solubilized proteins were separated from the insoluble fractions by ultracentrifugation at 142,000g for 1 h. The proteins were purified using a Co-NTA affinity column (HiTrap TALON crude; Cytiva). The resin was washed with buffer containing 50 mM MES-NaOH (pH 6.5), 300 mM NaCl, 50 mM imidazole, 5 mM MgCl₂, and 0.1% DDM. The proteins were eluted in a buffer containing 50 mM Tris-HCl (pH 7.0), 300 mM NaCl, 300 mM imidazole, 5 mM MgCl₂, and 0.1% DDM. The eluted proteins were dialyzed in buffer containing 20 mM Hepes-NaOH (pH 7.0), 100 mM NaCl, 0.05% DDM for crystallization, and 50 mM Tris-HCl (pH 8.0), 100 mM NaCl, and 0.05% DDM for laser flash photolysis to remove imidazole.

Crystallization of PspR

Concentrated PspR (34 mg/ml protein) was mixed with monoolein (Nu-Chek Prep) in a protein:lipid ratio of 2:3 (v/v) using the LCP method at 23 °C. The mixed sample was dispensed onto glass sandwich plates in a 50 nl drop and was overlaid with 800 nl of reservoir solution consisting of 0.1 M MgCl₂, 0.2 M NaCl, 0.1 M sodium citrate (pH 4.0), and 31% PEG-300 by Mosquito LCP (TTP Labtech Ltd). The crystals were harvested directly from the LCP bolus, flash-cooled, and stored in liquid nitrogen.

X-ray diffraction data collection and structure determination

X-ray diffraction data were collected from a single crystal at a cryogenic temperature (100 K) on BL-1A beamline ($\lambda = 1.0800 \text{ \AA}$) at the Photon Factory. The collected data were processed to 2.84 Å using XDS software (56). The structure was solved by molecular replacement with Molrep (57) as a search model for the homology model built using SWISS-MODEL (58) based on *Rubrobacter xylophilus* rhodopsin (Protein Data Bank ID: 6KFQ). The atomic model was built using Coot (59) and iteratively refined using the Phenix (60). Translation/libration/screw refinement was performed in the late stages of refinement. The refined structures were validated using the RAMPAGE (61).

Proton transport activity assay

E. coli cells expressing rhodopsins were collected by centrifugation (4800g, 2 min, 20 °C) (CF15RE; Eppendorf HimaC Technologies) and washed with unbuffered 100 mM NaCl. The cells were equilibrated three times with rotational mixing in unbuffered 100 mM NaCl for 10 min at room temperature. Finally, the cells were suspended in 7.5 ml of unbuffered 100 mM NaCl, and absorbance at 600 nm was adjusted to 2. The cell suspension was placed in the dark in a

glass cell at 20 °C and illuminated at $\lambda > 500 \text{ nm}$ from the output of a 300 W xenon light source (MAX-303; Asahi Spectra) through a long-pass filter (Y-52; AGC Techno Glass) and a heat-absorbing filter (HAF-50S-50H; SIGMAKOKI). Light-induced pH changes were measured using a pH electrode (9618S-10D; HORIBA). To evaluate the effect of light quality on the ion transport activity, a bandpass filter at $530 \pm 5 \text{ nm}$ (HQBP530-VIS; Asahi Spectra) was used instead of the Y-52 filter. The measurements were repeated under the same conditions after the addition of 10 μM carbonyl cyanide *m*-chlorophenylhydrazone. To quantitatively compare the ion transport activity, the amount of protein was determined by measuring the near-UV absorption of retinal oxime generated by the hydrolysis reaction between the RSB in the proteins and hydroxylamine. Briefly, *E. coli* cells expressing rhodopsins were washed with a solution containing 133 mM NaCl and 66.5 mM Na₂HPO₄ (pH 8). The washed cells were treated with 1 mM lysozyme and a small amount of DNaseI for 1 h and then disrupted by sonication. To solubilize rhodopsins, 3% DDM was added, and the samples were stirred overnight at 4 °C. The rhodopsins were bleached with 50 mM hydroxylamine and illuminated with visible light ($\lambda > 500 \text{ nm}$) from the output of a 300 W xenon lamp (MAX-303; Asahi Spectra) through a long-pass filter (Y-52; AGC Techno Glass) and a heat-absorbing filter (HAF-50S-50H). The absorption changes upon the bleaching of rhodopsin by the hydrolysis reaction between the retinal and hydroxylamine and the formation of retinal oxime were measured using a UV-visible spectrometer (V-750; JASCO). The molecular extinction coefficient of rhodopsin (ϵ) was calculated as the ratio between the absorbance of rhodopsin and retinal oxime ($\epsilon = 33,900 \text{ M}^{-1} \text{ cm}^{-1}$), and the amount of rhodopsin expressed in *E. coli* cells was determined by the absorbance of bleached rhodopsin and their ϵ . The relative ion transport activities were normalized to the relative amounts of expressed proteins.

Laser flash photolysis

The detail of laser flash photolysis system was previously reported (22, 62). PspR WT and mutants were purified and reconstituted into a mixture of 1-palmitoyl-2-oleoyl-phosphatidyl-ethanolamine (Avanti Polar Lipids) and 1-palmitoyl-2-oleoyl-*sn*-glycero-3-phosphoglycerol (sodium salt; Avanti Polar Lipids) (molar ratio = 3:1) with a protein-to-lipid molar ratio of 1:50 in 100 mM NaCl and 20 mM Hepes-NaOH (pH 7.0), and DDM was removed by Bio-Beads (SM-2; Bio-Rad). The buffer of the sample solution was exchanged with 6-mix buffer (10 mM trisodium citrate, 10 mM MES, 10 mM Hepes, 10 mM Mops, 10 mM Ches, 10 mM *N*-cyclohexyl-3-aminopropanesulfonic acid, and 650 mM NaCl) at different pH values (from pH 5 to 9) to determine the pH dependence of the photocycle. The absorption of the protein solution was adjusted to ~0.8 (total protein concentration of ~0.15 mg ml⁻¹) at an excitation wavelength of 532 nm. The sample was illuminated with a beam of second harmonics of a nanosecond-pulsed Nd:YAG laser ($\lambda = 532 \text{ nm}$, 5.7 mJ/cm², 0.025–1 Hz) (INDI40; Spectra-Physics). The time evolution of

X-ray crystallographic structure of DTG/DTS rhodopsin

the transient absorption change was obtained by observing the intensity change of the output of an Xe arc lamp (L9289-01; Hamamatsu Photonics), monochromated by a monochromator (S-10; SOMA OPTICS) and passed through the sample, after photoexcitation by a photomultiplier tube (R10699; Hamamatsu Photonics) equipped with a notch filter (532 nm, bandwidth = 17 nm) (Semrock) to remove the scattered pump pulse. To increase the signal-to-noise ratio, 100 to 200 signals were averaged. The signals were global fitted with a multiexponential function to determine the lifetimes of each photointermediate.

Data availability

Data supporting the findings are available from the corresponding authors upon reasonable request. The atomic coordinates and structure factors of *PspR* were deposited in the Protein Data Bank under the accession code 7W74 (<https://doi.org/10.2210/pdb7w74/pdb>).

Supporting information—This article contains supporting information.

Acknowledgments—We thank Prof Oded Bèjà and Dr Andrey Rozenberg for providing the genetic information on DTG/DTS rhodopsins. The synchrotron radiation experiments were performed at the Photon Factory (proposal 2020RP-14). We also thank the beamline staff at BL1A of the Photon Factory (Tsukuba, Japan) for their help during data collection.

Author contributions—T. M. and K. I. methodology; K. S., M. d. C. M., M. K., R. B., T. M., and K. I. investigation; K. S., T. M., and K. I. writing—original draft.

Funding and additional information—This work was supported by the Ministry of Education, Culture, Sports, Science and Technology KAKENHI, Grant-in-aid for Transformative Research Areas (B) “Low-energy manipulation” (grant number: JP20H05758; to K. I.), Japan Society for the Promotion of Science KAKENHI, Grants-in-aid (grant numbers: JP20F20081 [to M. d. C. M.], JP18H05425 [to T. M.], as well as JP21H01875 and JP20K21383 [to K. I.]), International Research Fellow of the Japan Society for the Promotion of Science (Postdoctoral Fellowships for Research in Japan; to M. d. C. M.), and the Japan Agency for Medical Research and Development (AMED) under grant no. 21fk0108092 to T. M.

Conflict of interest—The authors declare that they have no conflicts of interest with the contents of this article.

Abbreviations—The abbreviations used are: BR, bacteriorhodopsin; DDM, *n*-dodecyl- β -D-maltopyranoside; ES, extracellular side; LCP, lipidic cubic phase; PRG, proton-release group; *PspR*, DTG rhodopsin from *Pseudomonas putida*; RSB, retinal Schiff base; str., stretching; TM, transmembrane helix.

References

- Ernst, O. P., Lodowski, D. T., Elstner, M., Hegemann, P., Brown, L. S., and Kandori, H. (2014) Microbial and animal rhodopsins: Structures, functions, and molecular mechanisms. *Chem. Rev.* **114**, 126–163
- Govorunova, E. G., Sineshchekov, O. A., Li, H., and Spudich, J. L. (2017) Microbial rhodopsins: Diversity, mechanisms, and optogenetic applications. *Annu. Rev. Biochem.* **86**, 845–872
- Rozenberg, A., Inoue, K., Kandori, H., and Bèjà, O. (2021) Microbial rhodopsins: The last two decades. *Annu. Rev. Microbiol.* **75**, 427–447
- Philosof, A., Yutin, N., Flores-Urbe, J., Sharon, I., Koonin, E. V., and Bèjà, O. (2017) Novel abundant oceanic viruses of uncultured marine group II euryarchaeota. *Curr. Biol.* **27**, 1362–1368
- Rozenberg, A., Oppermann, J., Wietek, J., Fernandez Lahore, R. G., Sandaa, R. A., Bratbak, G., Hegemann, P., and Bèjà, O. (2020) Lateral gene transfer of anion-conducting channelrhodopsins between green algae and giant viruses. *Curr. Biol.* **30**, 4910–4920
- Inoue, K. (2021) Diversity, mechanism, and optogenetic application of light-driven ion pump rhodopsins. In: Yawo, H., Kandori, H., Koizumi, A., Kageyama, R., eds. *Optogenetics – Light-Sensing Proteins and Their Applications in Neuroscience and Beyond*, 2nd Ed, Springer Singapore, Singapore: 89–126
- Inoue, K., Kato, Y., and Kandori, H. (2014) Light-driven ion-translocating rhodopsins in marine bacteria. *Trends Microbiol.* **23**, 91–98
- Kato, H. E. (2021) Structure-function relationship of channelrhodopsins. In: Yawo, H., Kandori, H., Koizumi, A., Kageyama, R., eds. *Optogenetics – Light-Sensing Proteins and Their Applications in Neuroscience and Beyond*, Springer Singapore, Singapore: 35–53
- Deisseroth, K., and Hegemann, P. (2017) The form and function of channelrhodopsin. *Science* **357**, eaan5544
- Govorunova, E. G., and Koppel, L. A. (2016) The road to optogenetics: Microbial rhodopsins. *Biochemistry (Mosc.)* **81**, 928–940
- Jung, K. H., Trivedi, V. D., and Spudich, J. L. (2003) Demonstration of a sensory rhodopsin in eubacteria. *Mol. Microbiol.* **47**, 1513–1522
- Irieda, H., Morita, T., Maki, K., Homma, M., Aiba, H., and Sudo, Y. (2012) Photo-induced regulation of the chromatic adaptive gene expression by *Anabaena* sensory rhodopsin. *J. Biol. Chem.* **287**, 32485–32493
- Mukherjee, S., Hegemann, P., and Broser, M. (2019) Enzymerhodopsins: Novel photoregulated catalysts for optogenetics. *Curr. Opin. Struct. Biol.* **57**, 118–126
- Pushkarev, A., Inoue, K., Larom, S., Flores-Urbe, J., Singh, M., Konno, M., Tomida, S., Ito, S., Nakamura, R., Tsunoda, S. P., Philosof, A., Sharon, I., Yutin, N., Koonin, E. V., Kandori, H., et al. (2018) A distinct abundant group of microbial rhodopsins discovered using functional metagenomics. *Nature* **558**, 595–599
- Racker, E., and Stoerckenius, W. (1974) Reconstitution of purple membrane vesicles catalyzing light-driven proton uptake and adenosine triphosphate formation. *J. Biol. Chem.* **249**, 662–663
- Oesterhelt, D., and Stoerckenius, W. (1971) Rhodopsin-like protein from the purple membrane of *Halobacterium halobium*. *Nat. New Biol.* **233**, 149–152
- Lanyi, J. K. (2004) Bacteriorhodopsin. *Annu. Rev. Physiol.* **66**, 665–688
- Garczarek, F., and Gerwert, K. (2006) Functional waters in intraprotein proton transfer monitored by FTIR difference spectroscopy. *Nature* **439**, 109–112
- Lórenz-Fonfría, V. A., and Kandori, H. (2009) Spectroscopic and kinetic evidence on how bacteriorhodopsin accomplishes vectorial proton transport under functional conditions. *J. Am. Chem. Soc.* **131**, 5891–5901
- Dioumaev, A. K., Brown, L. S., Needleman, R., and Lanyi, J. K. (1999) Fourier transform infrared spectra of a late intermediate of the bacteriorhodopsin photocycle suggest transient protonation of Asp-212. *Biochemistry* **38**, 10070–10078
- Zscherp, C., Schlesinger, R., and Heberle, J. (2001) Time-resolved FT-IR spectroscopic investigation of the pH-dependent proton transfer reactions in the E194Q mutant of bacteriorhodopsin. *Biochem. Biophys. Res. Commun.* **283**, 57–63
- Inoue, K., Ono, H., Abe-Yoshizumi, R., Yoshizawa, S., Ito, H., Kogure, K., and Kandori, H. (2013) A light-driven sodium ion pump in marine bacteria. *Nat. Commun.* **4**, 1678
- Bèjà, O., Aravind, L., Koonin, E. V., Suzuki, M. T., Hadd, A., Nguyen, L. P., Jovanovich, S. B., Gates, C. M., Feldman, R. A., Spudich, J. L., Spudich, E. N., and DeLong, E. F. (2000) Bacterial rhodopsin: Evidence for a new type of phototrophy in the sea. *Science* **289**, 1902–1906

24. Balashov, S. P., Imasheva, E. S., Boichenko, V. A., Anton, J., Wang, J. M., and Lanyi, J. K. (2005) Xanthorhodopsin: A proton pump with a light-harvesting carotenoid antenna. *Science* **309**, 2061–2064
25. Balashov, S. P., Petrovskaya, L. E., Imasheva, E. S., Lukashev, E. P., Dioumaev, A. K., Wang, J. M., Sychev, S. V., Dolgikh, D. A., Rubin, A. B., Kirpichnikov, M. P., and Lanyi, J. K. (2013) Breaking the carboxyl rule: Lysine 96 facilitates reprotonation of the Schiff base in the photocycle of a retinal protein from *Exiguobacterium sibiricum*. *J. Biol. Chem.* **288**, 21254–21265
26. Harris, A., Ljumovic, M., Bondar, A. N., Shibata, Y., Ito, S., Inoue, K., Kandori, H., and Brown, L. S. (2015) A new group of eubacterial light-driven retinal-binding proton pumps with an unusual cytoplasmic proton donor. *Biochim. Biophys. Acta* **1847**, 1518–1529
27. Sudo, Y., and Yoshizawa, S. (2016) Functional and photochemical characterization of a light-driven proton pump from the gammaproteobacterium *Pantoea vagans*. *Photochem. Photobiol.* **92**, 420–427
28. Maliar, N., Okhrimenko, I. S., Petrovskaya, L. E., Alekseev, A. A., Kovalev, K. V., Soloviov, D. V., Popov, P. A., Rokitskaya, T. I., Antonenko, Y. N., Zabelskii, D. V., Dolgikh, D. A., Kirpichnikov, M. P., and Gordeliy, V. I. (2020) Novel pH-sensitive microbial rhodopsin from *Sphingomonas paucimobilis*. *Dokl. Biochem. Biophys.* **495**, 342–346
29. Dioumaev, A. K., Wang, J. M., Balint, Z., Varo, G., and Lanyi, J. K. (2003) Proton transport by proteorhodopsin requires that the retinal Schiff base counterion Asp-97 be anionic. *Biochemistry* **42**, 6582–6587
30. Luecke, H., Schobert, B., Stagno, J., Imasheva, E. S., Wang, J. M., Balashov, S. P., and Lanyi, J. K. (2008) Crystallographic structure of xanthorhodopsin, the light-driven proton pump with a dual chromophore. *Proc. Natl. Acad. Sci. U. S. A.* **105**, 16561–16565
31. Miranda, M. R., Choi, A. R., Shi, L., Bezerra, A. G., Jr., Jung, K. H., and Brown, L. S. (2009) The photocycle and proton translocation pathway in a cyanobacterial ion-pumping rhodopsin. *Biophys. J.* **96**, 1471–1481
32. Wada, T., Shimono, K., Kikukawa, T., Hato, M., Shinya, N., Kim, S. Y., Kimura-Someya, T., Shirouzu, M., Tamogami, J., Miyauchi, S., Jung, K. H., Kamo, N., and Yokoyama, S. (2011) Crystal structure of the eukaryotic light-driven proton-pumping rhodopsin, *Acetabularia* rhodopsin II, from marine alga. *J. Mol. Biol.* **411**, 986–998
33. Vogt, A., Guo, Y., Tsunoda, S. P., Kateriya, S., Elstner, M., and Hegemann, P. (2015) Conversion of a light-driven proton pump into a light-gated ion channel. *Sci. Rep.* **5**, 16450
34. Needham, D. M., Yoshizawa, S., Hosaka, T., Poirier, C., Choi, C. J., Hehenberger, E., Irwin, N. A. T., Wilken, S., Yung, C. M., Bachy, C., Kurihara, R., Nakajima, Y., Kojima, K., Kimura-Someya, T., Leonard, G., et al. (2019) A distinct lineage of giant viruses brings a rhodopsin photosystem to unicellular marine predators. *Proc. Natl. Acad. Sci. U. S. A.* **116**, 20574–20583
35. Sass, H. J., Büldt, G., Gessenich, R., Hehn, D., Neff, D., Schlesinger, R., Berendzen, J., and Ormos, P. (2000) Structural alterations for proton translocation in the M state of wild-type bacteriorhodopsin. *Nature* **406**, 649–653
36. Subramaniam, S., Greenhalgh, D. A., Rath, P., Rothschild, K. J., and Khorana, H. G. (1991) Replacement of leucine-93 by alanine or threonine slows down the decay of the N and O intermediates in the photocycle of bacteriorhodopsin: Implications for proton uptake and 13-*cis*-retinal→all-*trans*-retinal reversion. *Proc. Natl. Acad. Sci. U. S. A.* **88**, 6873–6877
37. Luecke, H., Schobert, B., Richter, H. T., Cartailler, J. P., and Lanyi, J. K. (1999) Structure of bacteriorhodopsin at 1.55 Å resolution. *J. Mol. Biol.* **291**, 899–911
38. Nango, E., Royant, A., Kubo, M., Nakane, T., Wickstrand, C., Kimura, T., Tanaka, T., Tono, K., Song, C., Tanaka, R., Arima, T., Yamashita, A., Kobayashi, J., Hosaka, T., Mizohata, E., et al. (2016) A three-dimensional movie of structural changes in bacteriorhodopsin. *Science* **354**, 1552–1557
39. Higuchi, A., Shihoya, W., Konno, M., Ikuta, T., Kandori, H., Inoue, K., and Nureki, O. (2021) Crystal structure of schizorhodopsin reveals mechanism of inward proton pumping. *Proc. Natl. Acad. Sci. U. S. A.* **118**, e2016328118
40. Shibata, M., Inoue, K., Ikeda, K., Konno, M., Singh, M., Kataoka, C., Abe-Yoshizumi, R., Kandori, H., and Uchihashi, T. (2018) Oligomeric states of microbial rhodopsins determined by high-speed atomic force microscopy and circular dichroic spectroscopy. *Sci. Rep.* **8**, 8262
41. Besaw, J. E., Ou, W. L., Morizumi, T., Eger, B. T., Sanchez Vasquez, J. D., Chu, J. H. Y., Harris, A., Brown, L. S., Miller, R. J. D., and Ernst, O. P. (2020) The crystal structures of a chloride-pumping microbial rhodopsin and its proton-pumping mutant illuminate proton transfer determinants. *J. Biol. Chem.* **295**, 14793–14804
42. Zabelskii, D., Dmitrieva, N., Volkov, O., Shevchenko, V., Kovalev, K., Balandin, T., Soloviov, D., Astashkin, R., Zinovev, E., Alekseev, A., Round, E., Polovinkin, V., Chizhov, I., Rogachev, A., Okhrimenko, I., et al. (2021) Structure-based insights into evolution of rhodopsins. *Commun. Biol.* **4**, 821
43. Fudim, R., Szczepek, M., Vierock, J., Vogt, A., Schmidt, A., Kleinau, G., Fischer, P., Bartl, F., Scheerer, P., and Hegemann, P. (2019) Design of a light-gated proton channel based on the crystal structure of *Coccomyxa* rhodopsin. *Sci. Signal.* **12**, eaav4203
44. Kandori, H. (2020) Structure/function study of photoreceptive proteins by FTIR spectroscopy. *Bull. Chem. Soc. Jpn.* **93**, 904–926
45. Shibata, M., Tanimoto, T., and Kandori, H. (2003) Water molecules in the Schiff base region of bacteriorhodopsin. *J. Am. Chem. Soc.* **125**, 13312–13313
46. Subramaniam, S., and Henderson, R. (2000) Molecular mechanism of vectorial proton translocation by bacteriorhodopsin. *Nature* **406**, 653–657
47. Rink, T., Pfeiffer, M., Oesterheld, D., Gerwert, K., and Steinhoff, H. J. (2000) Unraveling photoexcited conformational changes of bacteriorhodopsin by time resolved electron paramagnetic resonance spectroscopy. *Biophys. J.* **78**, 1519–1530
48. Shibata, M., Yamashita, H., Uchihashi, T., Kandori, H., and Ando, T. (2010) High-speed atomic force microscopy shows dynamic molecular processes in photoactivated bacteriorhodopsin. *Nat. Nanotechnol.* **5**, 208–212
49. Otto, H., Marti, T., Holz, M., Mogi, T., Lindau, M., Khorana, H. G., and Heyn, M. P. (1989) Aspartic acid-96 is the internal proton donor in the reprotonation of the Schiff base of bacteriorhodopsin. *Proc. Natl. Acad. Sci. U. S. A.* **86**, 9228–9232
50. Padan, E., Bibi, E., Ito, M., and Krulwich, T. A. (2005) Alkaline pH homeostasis in bacteria: New insights. *Biochim. Biophys. Acta* **1717**, 67–88
51. Donahue, C. E. T., Siroky, M. D., and White, K. A. (2021) An optogenetic tool to raise intracellular pH in single cells and drive localized membrane dynamics. *J. Am. Chem. Soc.* **143**, 18877
52. Thompson, J. D., Higgins, D. G., and Gibson, T. J. (1994) Clustal-W - improving the sensitivity of progressive multiple sequence alignment through sequence weighting, position-specific gap penalties and weight matrix choice. *Nucleic Acids Res.* **22**, 4673–4680
53. Saitou, N., and Nei, M. (1987) The neighbor-joining method: A new method for reconstructing phylogenetic trees. *Mol. Biol. Evol.* **4**, 406–425
54. Zuckerkandl, E., and Pauling, L. (1965) Evolutionary divergence and convergence in proteins. In: Bryson, V., Vogel, H. J., eds. *Evolving Genes and Proteins*, Academic Press, New York, NY: 97–166
55. Tamura, K., Peterson, D., Peterson, N., Stecher, G., Nei, M., and Kumar, S. (2011) Mega5: Molecular evolutionary genetics analysis using maximum likelihood, evolutionary distance, and maximum parsimony methods. *Mol. Biol. Evol.* **28**, 2731–2739
56. Kabsch, W. (2010) XDS. *Acta Crystallogr. D Biol. Crystallogr.* **66**, 125–132
57. Vagin, A., and Teplyakov, A. (2010) Molecular replacement with MOLREP. *Acta Crystallogr. D Biol. Crystallogr.* **66**, 22–25
58. Waterhouse, A., Bertoni, M., Bienert, S., Studer, G., Tauriello, G., Gumienny, R., Heer, F. T., de Beer, T. A. P., Rempfer, C., Bordoli, L., Lepore, R., and Schwede, T. (2018) Swiss-model: Homology modelling of protein structures and complexes. *Nucleic Acids Res.* **46**, W296–W303
59. Emsley, P., and Cowtan, K. (2004) Coot: Model-building tools for molecular graphics. *Acta Crystallogr. D Biol. Crystallogr.* **60**, 2126–2132
60. Adams, P. D., Afonine, P. V., Bunkoczi, G., Chen, V. B., Davis, I. W., Echols, N., Headd, J. J., Hung, L. W., Kapral, G. J., Grosse-Kunstleve, R. W., McCoy, A. J., Moriarty, N. W., Oeffner, R., Read, R. J., Richardson, D. C., et al. (2010) Phenix: A comprehensive Python-based system for macromolecular structure solution. *Acta Crystallogr. D Biol. Crystallogr.* **66**, 213–221

X-ray crystallographic structure of DTG/DTS rhodopsin

61. Lovell, S. C., Davis, I. W., Arendall, W. B., 3rd, de Bakker, P. I., Word, J. M., Prisant, M. G., Richardson, J. S., and Richardson, D. C. (2003) Structure validation by calpha geometry: ϕ, ψ and $C\beta$ deviation. *Proteins* **50**, 437–450
62. Inoue, K., Tsunoda, S. P., Singh, M., Tomida, S., Hososhima, S., Konno, M., Nakamura, R., Watanabe, H., Bulzu, P. A., Banciu, H. L., Andrei, A., Uchihashi, T., Ghai, R., Béjà, O., and Kandori, H. (2020) Schizorhodopsins: A family of rhodopsins from asgard archaea that function as light-driven inward H^+ pumps. *Sci. Adv.* **6**, eaaz2441
63. Schobert, B., Cupp-Vickery, J., Hornak, V., Smith, S., and Lanyi, J. (2002) Crystallographic structure of the K intermediate of bacteriorhodopsin: Conservation of free energy after photoisomerization of the retinal. *J. Mol. Biol.* **321**, 715–726